# Operational parameter impact and back propagation artificial neural network modeling for phosphate adsorption onto acid-activated neutralized red mud

Jie Ye [a,b,c], Xiangna Cong [d], Panyue Zhang [a,b,*], Guangming Zeng [a,b,*], Erhard Hoffmann [c], Yan Wu [a,b], Haibo Zhang [a,b], Wei Fang [a,b]

[a] College of Environmental Science and Engineering, Hunan University, Changsha 410082, PR China
[b] Key Laboratory of Environmental Biology and Pollution Control (Hunan University), Ministry of Education, Changsha 410082, PR China
[c] Department of Aquatic Environmental Engineering, Karlsruhe Institute of Technology, Karlsruhe D-76131, Germany
[d] The Institute for Applied Materials IAM-WK, Karlsruhe Institute of Technology, Karlsruhe D-76131, Germany

## ARTICLE INFO

## ABSTRACT

In this research the combination of neutralization activation and acid activation processes was employed to improve the physicochemical characters of red mud. In order to better understand the phosphate adsorption behaviors and further improve the phosphate adsorption performance of acid-activated neutralized red mud (AaN-RM), for the first time the impact of operational parameters on phosphate adsorption onto AaN-RM was systematically investigated, and back propagation artificial neural network (ANN) modeling was conducted. The results demonstrated that phosphate adsorption capacity of AaN-RM decreased with the enhancement of adsorbent dosage and the concentration of the competing ion (carbonate), while it increased with the increase of initial phosphate concentration and contact time. The optimal adsorption temperature and initial solution pH for phosphate adsorption onto AaN-RM were 50 °C and 4.0, respectively. Moreover, a 6-10-1 feed forward ANN structure with trainlm algorithm was successfully constructed for predicting the phosphate removal by AaN-RM. The RMSE and $R^2$ values for two subsets (training and validation subset, and testing subset) were 3.06 and 2.61, and 0.9932 and 0.9969, respectively. Furthermore, the importance analysis showed that contact time and initial phosphate concentration were the most influential parameters on phosphate removal by AaN-RM, the importance of which reached 24.64% and 22.16%, respectively.

© 2016 Elsevier B.V. All rights reserved.

## 1. Introduction

Phosphorus is a non-renewable macronutrient for the growth of plants and other organisms in the ecosystem [1]. However, the excessive discharge of phosphorus into water bodies may cause detrimental eutrophication, which not only seriously destroy the biodiversity but also threaten the drinking water safety [2]. Therefore, it is necessary to explore effective methods to remove and recover phosphate from municipal and industrial wastewater. Compared with other available technologies, the adsorption method has incomparable advantages due to its inexpensiveness, simplicity of design, ease of operation, and insensitivity to toxic pollutants [3]. Various natural minerals, industrial by-products and synthetic adsorbents have been used in phosphate adsorption systems [4]. Among these available materials, red mud is considered to be a promising alternative [5,6].

Red mud, a waste tailing generated from the alumina producing process, is a hazardous solid waste because of its highly alkaline nature [7]. There are three processes commercially applied for alumina refining, including the sintering process, the Bayer process, and the combination process (Bayer-sintering) [8]. Among them, the Bayer process is a key method used in producing quality alumina worldwide. It was reported that about 90% of bauxite is processed by Bayer technology [9]. Correspondingly, managing the rapidly expanding Bayer red mud, a hazardous solid waste generated in alumina refining from bauxite with Bayer technology, has become more and more important. Up to date, Bayer red mud has got a variety of applications such as adsorbents, catalysts and coagulants [10], and the application of modified red mud in wastewater treatment has become an emerging and promising research field [11–13]. However, most works only employed single activation technology such as acid activation or heat activation to improve the physicochemical characters of red mud [14–15]. Our previous study demonstrated that the combination of neutralization activation and acid activation technologies effectively improved the phosphate adsorption capacity of red mud [16]. In order to better understand the phosphate adsorption behaviors and further improve the phosphate

* Corresponding authors at: College of Environmental Science and Engineering, Hunan University, Yuelushan, Changsha 410082, PR China.
E-mail addresses: zhangpanyue@hnu.edu.cn (P. Zhang), zgming@hnu.cn (G. Zeng).

adsorption performance of acid-activated neutralized red mud (AaN-RM), the effects of different operational parameters should be systematically investigated.

Nowadays, the application of artificial neural network (ANN) for mapping, regression, modeling, clustering, classification and multivariate data analysis has attracted increasing attention [17,18]. The ANN is a multivariate statistics technique which is commonly used to describe a variety of mathematical objects and processes [19]. The main advantages of ANN include nonlinearity, allowing better fit to the data; noise insensitivity, providing accurate prediction in the presence of uncertain data and measurement errors; high parallelism, which implies fast processing and hardware failure tolerance; learning and adaptability, allowing the system to update (modify) its internal structure in response to changing environment and generalization [20]. Feed forward back propagation network is the most widely used ANN architecture, which is suitable for modeling the whole phosphate adsorption process and evaluating the importance of different operational parameters [21, 22].

Therefore, the aims of this study were: (1) investigating the effects of different operational parameters on phosphate adsorption onto AaN-RM; (2) evaluating the potential of back propagation artificial neural network for modeling the phosphate adsorption performance of AaN-RM with different training algorithms; (3) quantifying the importance of different operational parameters on the phosphate adsorption process.

## 2. Materials and methods

### 2.1. Materials

The Bayer red mud was provided by Shandong Aluminum Industry Corporation (Zibo, China), and the preparation method of AaN-RM can be found in [16]. The phosphate and carbonate solutions were prepared by potassium dihydrogen phosphate and sodium carbonate, respectively. All chemicals were of analytical grade (Merck Co., Germany).

### 2.2. Characterization of AaN-RM

The surface micro-morphology of AaN-RM was analyzed with electron dispersive X-ray analysis (Oxford X-Max, Oxford Instruments, UK), which was coupled with an electronic detector (LEO 1530, LEO, Germany). With $N_2$ adsorption/desorption isotherms at 77 K, the Brunauer–Emmett–Teller (BET) surface area and total pore volume of the samples were determined (ASAP 2020 V3.04 H, Micromeritics, USA). The chemical composition of AaN-RM was determined by X-ray fluorescence spectrometer (S4 Explorer, Bruker, Germany). The XRD patterns of AaN-RM were detected using an X-ray diffractometer (XRD-6000, Shimadzu, Japan) with Cu Kα radiation at 40 kV and 30 mA, and recorded in a $2\theta$ range of 10–70° at a scan speed range of 0.02°/s. The point of zero charge ($pH_{pzc}$) of AaN-RM was estimated by batch equilibrium techniques described by Chutia et al. [23].

**Table 1**
Choice of operational parameters for optimization and ANN analysis.

| ANN structure | Operational parameters | Range |
|---|---|---|
| Input parameters | Adsorbent dosage (mg/g) | 0.3–0.8 |
| | Initial solution pH | 2.0–6.0 |
| | Adsorption temperature (°C) | 20–70 |
| | Initial phosphate concentration (mg/L) | 20–200 |
| | Contact time (min) | 0–20 |
| | Competing ion (carbonate) (mg/L) | 0–206.8 |
| Output parameters | Phosphate adsorption capacity (mg/g) | 31.34–192.62 |
| Total number of data points | | 33 |

**Table 2**
ANN training parameters.

| Parameter | Value |
|---|---|
| Maximum number of epochs | 1000 |
| Learning rate | 0.1 |
| Momentum constant | 0.5 |
| Error goal | 0.0001 |

### 2.3. Adsorption studies

A series of phosphate solutions with different pH values were prepared with 1 mol/L and 0.1 mol/L HCl or NaOH solution. As shown in Table 1, the influences of different operational parameters on the phosphate adsorption performance of AaN-RM were investigated in beaker flasks. The parameters included adsorbent dosage, initial solution pH, adsorption temperature, initial phosphate concentration, contact time and competing ion. The beaker flasks were shaken at 100 rmp for 20 min. The samples were taken at predetermined time intervals, centrifuged at 3000 rmp for 1 min, and then the supernatant was taken to analyze the phosphate concentration.

The phosphate adsorbed by per unit of adsorbent was calculated by Eq. (1):

$$q = \frac{(C_i - C_f) \cdot V}{m} \tag{1}$$

where $q$ is the phosphate adsorption capacity per unit of AaN-RM (mg/g, as $PO_4^{3-}$), $C_i$ and $C_f$ are the initial and final phosphate concentration (mg/L), respectively, $V$ is the solution volume (L), and $m$ is the mass of adsorbent (g).

The pH value was measured with a multimeter (model Multiline P4, WTW, Germany). The phosphate concentration was determined via the spectrophotometric method DIN-EN-ISO-15681-1 with a QuikChem 8500 flow injection analysis system (Lachat Instruments, USA). All experiments were conducted in triplicate and the average values were used for data analysis.

### 2.4. ANN modeling

In this research a three-layer feed-forward neural network with back propagation learning was constructed for the modeling of phosphate adsorption onto AaN-RM with MATLAB 10.0. A tangent sigmoid transfer function (tansig) at the hidden layer and a linear transfer function (purelin) at the output layer were selected. Meanwhile, three kinds of training algorithms including training BFGS quasi-Newton
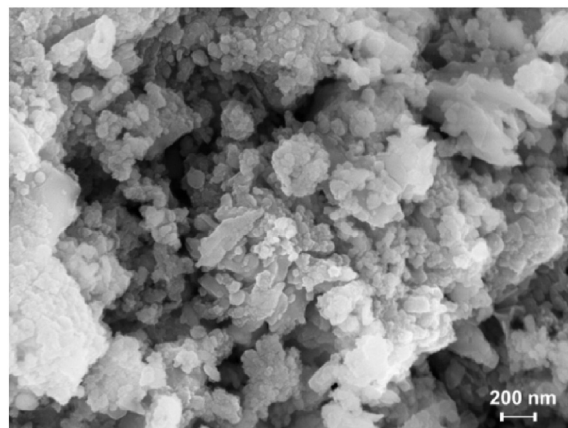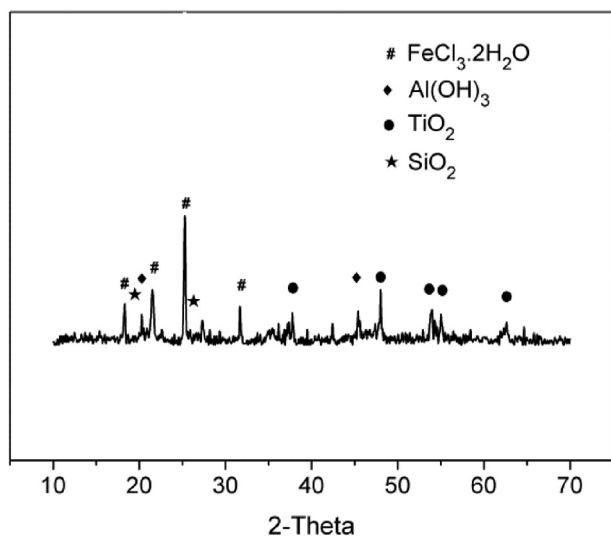


**Fig. 1.** SEM image of AaN-RM.
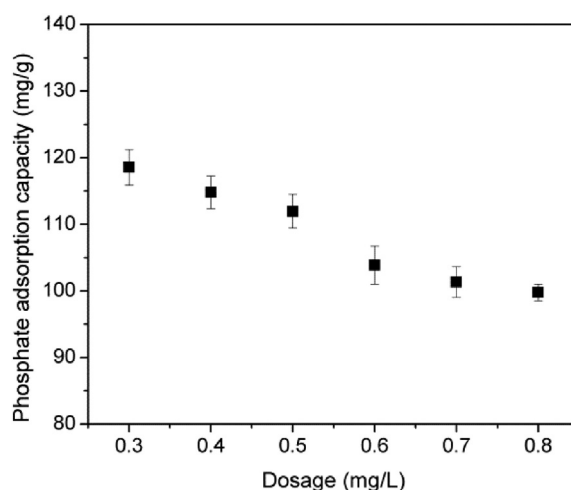
**Fig. 2.** XRD patterns of AaN-RM.



**Fig. 3.** Effect of adsorbent dosage on phosphate adsorption performance of AaN-RM (adsorption temperature: 20 °C; initial solution pH: 7.0; initial phosphate concentration: 200 mg/L; contact time: 20 min).

backpropagation algorithm (trainbfg), scaled conjugate gradient algorithm (trainscg) and Levenberg–Marquardt algorithm (trainlm) were implemented. The optimum ANN training parameters for three different training algorithms were shown in Table 2. As shown in Table 1, six parameters including adsorbent dosage, initial solution pH, adsorption temperature, initial phosphate concentration, contact time and competing ion were chosen as input layers.

The results were expressed in one neuron as phosphate adsorption capacity in the output layer. All the experimental data were normalized in the range of 0–1. Data ($x_i$) are converted to normalized value ($x_{normal}$) as follows [24]:

$$x_{normal} = \frac{0.8(x_i - x_{min})}{x_{max} - x_{min}} + 0.1 \tag{2}$$

where $x_{max}$ and $x_{min}$ are the maximum and minimum actual experimental data, respectively.

The performance of ANN with different algorithms was determined based on the values of root mean squared error (RMSE) and coefficient of determination ($R^2$). They were respectively calculated by Eqs. (3, 4) [25]:

$$RMSE = \left( \frac{1}{n} \sum_{i=1}^{n} (y_i - y_{di})^2 \right)^{1/2} \tag{3}$$

$$R^2 = \frac{\left( \sum_{i=1}^{n} (y_{di} - y_{di'})(y_i - y_{i'}) \right)^2}{\sum_{i=1}^{n} (y_{di} - y_{di'})^2 (y_i - y_{i'}))^2} \tag{4}$$

where the symbol ′ represents the average of related values, n is the number of points, $y_i$ is the predicted value and $y_{di}$ is the measured value.

The importance of each input variable in the ANN model in this study was calculated by Eq. (5) [26]:

$$I_i = \frac{\sum_{j=1}^{n_h} ABS(w_{ji})}{\sum_{k=1}^{n_v} \left( \sum_{j=1}^{n_h} ABS(w_{ji}) \right)_k} \tag{5}$$

where $n_h$ is the number of hidden nodes, $n_v$ is the number of input variables, $w_{ji}$ is the connection weight from the $i$th input node to the $j$th hidden node, and ABS denotes the absolute value of function.

## 3. Results and discussion
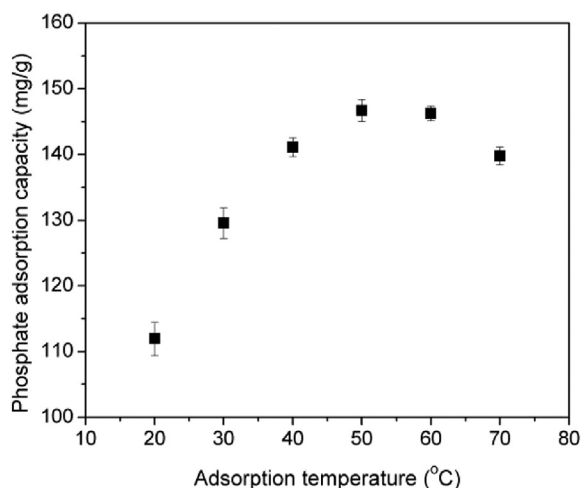
### 3.1. Characterization of the adsorbents

The SEM image of AaN-RM is shown in Fig. 1, which clearly revealed the rough and porous surface of AaN-RM. With BET $N_2$ adsorption–desorption analysis, it was found that the BET surface area and total pore volume of AaN-RM reached 80.63 $m^2$/g and 0.064 $cm^3$/g, respectively. X-ray diffraction patterns of AaN-RM in Fig. 2 presented specific chemical composition diffraction peaks at different $2\theta$ (°), indicating the presence of ferric chloride hydrate ($FeCl_3 \cdot 2H_2O$), gibbsite ($Al(OH)_3$), anatase ($TiO_2$) and quartz ($SiO_2$). The chemical composition of AaN-RM is listed in Table 3, which showed that Fe and Al oxides were the main components.

### 3.2. Effect of operational parameters on phosphate adsorption performance of AaN-RM

#### 3.2.1. Effect of adsorbent dosage

Adsorbent dosage could influence the phosphate removal from aqueous solutions. An increase in the adsorbent dosage could result in more reactive sites, which in turn improves the removal efficiency [27]. However, it should be pointed out that the increasing adsorbent dosage for a given amount of adsorbates would lead to unsaturation of adsorption sites, and then result in the decrease of adsorption capacity.

**Table 3**
Chemical composition of AaN-RM.

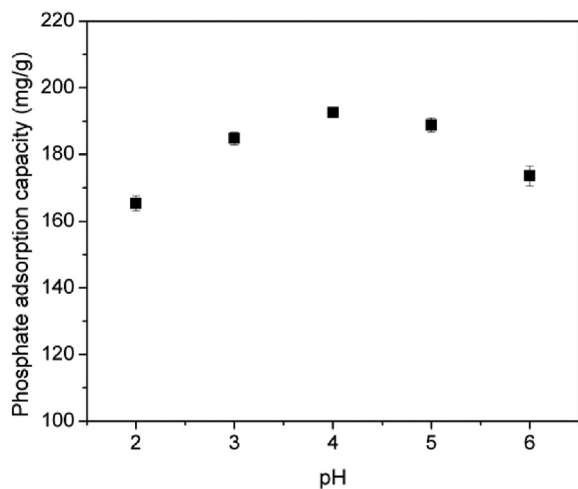| Constituent | $Fe_2O_3$ | $Al_2O_3$ | $SiO_2$ | $TiO_2$ | $Na_2O$ | CaO | $Cr_2O_3$ | MgO | $K_2O$ | MnO | NiO | CuO |
|---|---|---|---|---|---|---|---|---|---|---|---|---|
| (wt.%) | 33.88 | 30.96 | 15.52 | 14.69 | 3.83 | 0.54 | 0.22 | 0.17 | 0.10 | 0.06 | 0.02 | 0.01 |

**Fig. 4.** Effect of adsorption temperature on phosphate adsorption performance of AaN-RM (adsorbent dosage: 0.5 g/L; initial solution pH: 7.0; initial phosphate concentration: 200 mg/L; contact time: 20 min).



**Fig. 6.** The effect of initial phosphate concentration and contact time on phosphate adsorption performance of AaN-RM (adsorbent dosage: 0.5 g/L; adsorption temperature: 50 °C; initial solution pH: 4.0).
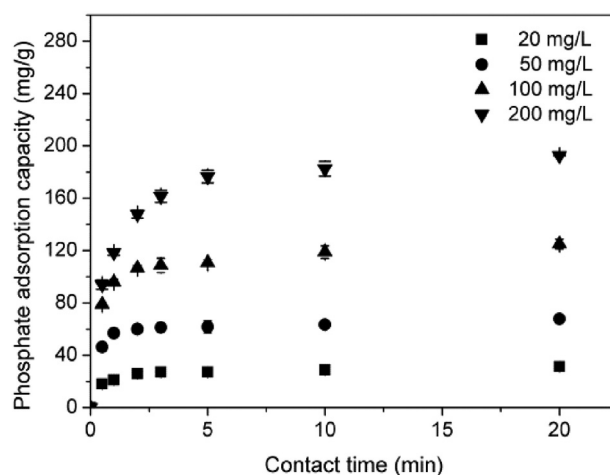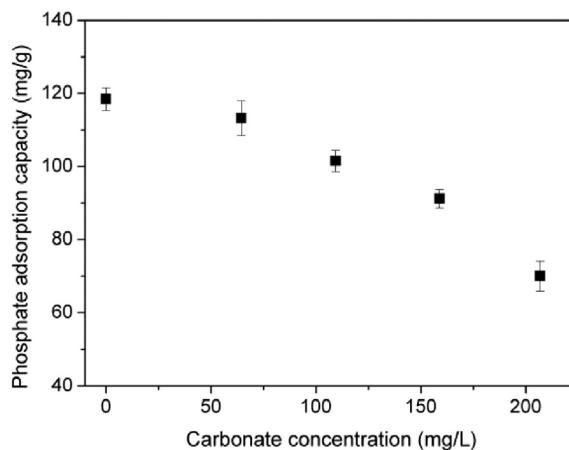
This would influence the cost and practicability of the adsorption system [28]. The influence of adsorbent dosage on phosphate adsorption capacity of AaN-RM is shown in Fig. 3. When the adsorbent dosage increased from 0.3 g/L to 0.8 g/L, the phosphate adsorption capacity of AaN-RM decreased from 121.56 mg/g to 99.75 mg/g, which demonstrated that phosphate adsorption capacity had negative correlation with adsorbent dosage. Babatunde et al. [29] found a similar conclusion, and attributed the main results to the increase of collision probability between different adsorbent particles with increasing adsorbent dosage. It reduced the efficient utilization of functional groups on adsorbent surface, and then influenced the adsorption performance.

### 3.2.2. Effect of adsorption temperature

Fig. 4 shows the phosphate adsorption capacity of AaN-RM as a function of different adsorption temperatures. It was found that the phosphate adsorption capacity of AaN-RM increased with the increase of adsorption temperature. However, when adsorption temperature was higher than 50 °C, the phosphate adsorption capacity of AaN-RM decreased slightly. This might be because the stability of AaN-RM was influenced by the higher temperature, which would further result in the decrease of phosphate adsorption capacity. The influence of

adsorption temperature on the performances of various adsorbents was different. Liu et al. [30] found that adsorption temperature showed positive influence on the phosphate adsorption capacity of lanthanum-doped activated carbon fiber within the temperature range of 20–50 °C. Yang et al. [31] also demonstrated that the phosphate adsorption process by lake sediments amended with zirconium-modified zeolites was favored at higher reaction temperature. However, Riebe et al. [32] illustrated that with an adsorption temperature of 20–60 °C, the iodide adsorption performance of organo-clay minerals decreased slightly with increasing temperature. This phenomenon could be explained by the thermodynamic and entropic effects of different adsorption processes [33].

### 3.2.3. Effect of initial solution pH

Initial solution pH could significantly influence the phosphate adsorption capacity of AaN-RM. As shown in Fig. 5, with the increase of solution pH, the phosphate adsorption capacity of AaN-RM increased firstly, and then decreased. When pH was 4.0, the maximum phosphate adsorption capacity of AaN-RM reached 192.62 mg/g. It is similar to that reported for the chromium (VI), arsenic (III) and arsenic (V) adsorption from an aqueous solution onto the activated red mud [34,35]. The point of zero charge ($pH_{pzc}$) for AaN-RM was about 5.9. When pH value



**Fig. 5.** Effect of initial solution pH on phosphate adsorption performance of AaN-RM (adsorbent dosage: 0.5 g/L; adsorption temperature: 50 °C; initial phosphate concentration: 200 mg/L; contact time: 20 min).



**Fig. 7.** Effect of competing ion (carbonate) on phosphate adsorption performance of AaN-RM (dosage: 0.5 g/L; adsorption temperature: 50 °C; initial solution pH: 8.0; contact time: 20 min).
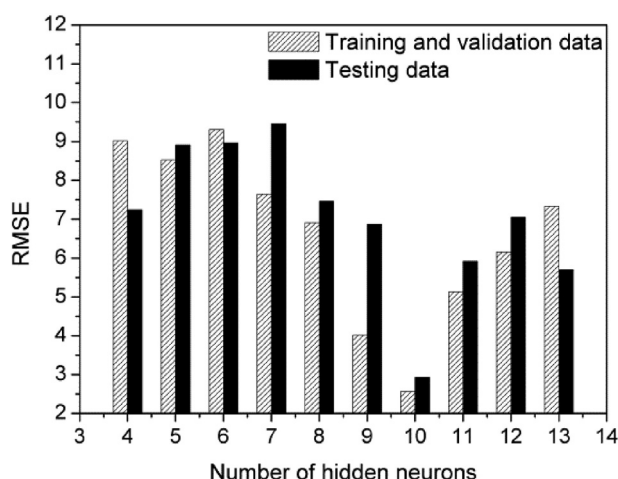
**Fig. 8.** Root mean square error (RMSE) for the different number of hidden neurons in ANN.

**Table 4**
The performance of ANN with different training algorithms.

| Training algorithms | Data category | Date sample | RMSE | $R^2$ |
|---|---|---|---|---|
| Trainbfg | Training and validation | 25 | 19.86 | 0.8134 |
|  | Testing | 8 | 17.10 | 0.9170 |
| Trainscg | Training and validation | 25 | 19.36 | 0.8264 |
|  | Testing | 8 | 18.90 | 0.8369 |
| Trainlm | Training and validation | 25 | 3.06 | 0.9932 |
|  | Testing | 8 | 2.61 | 0.9969 |

was lower than $pH_{pzc}$, the surface of AaN-RM was protonated, which effectively facilitated electrostatic attraction between the positive charged surface group and phosphate. However, if pH was too low, phosphoric acid ($H_3PO_4$) was the main existence form, which was not as active as $H_2PO_4^-$ and $HPO_4^{2-}$ to the adsorption sites, and then the phosphate adsorption performance would be restricted [36].

### 3.2.4. Effect of initial phosphate concentration and contact time

The effect of initial phosphate concentration and contact time on the phosphate adsorption capacity of AaN-RM is shown in Fig. 6. The results demonstrated that the phosphate adsorption capacity of AaN-RM increased dramatically from 31.34 mg/g to 192.62 mg/g with an increase in initial phosphate concentration from 20 mg/L to 200 mg/L. A higher concentration gradient acting as a driving force overcame the mass transfer resistance between the solution and adsorbent surface [30]. Meanwhile, as shown in Fig. 6, with different initial phosphate concentrations, the phosphate adsorption process always occurred very rapidly firstly, and then followed a slow process until adsorption equilibrium. When initial phosphate concentrations were 20, 50, 100 and 200 mg/L, the phosphate adsorption capacity of AaN-RM accounted for 86.60%, 91.01%, 88.57% and 91.63% of the total phosphate adsorption capacity within 5 min, respectively. This could be explained by the reason that the sufficient adsorption sites on the AaN-RM surface and the

available driving force for mass transfer were provided at the initial stage of adsorption [37].

### 3.2.5. Effect of competing ion

A variety of different anions in natural environments could affect the phosphate adsorption capacity of the adsorbent [38]. It has been reported that the phosphate adsorption capacity of ammonium-functionalized mobil composite material no. 48 increased slightly in the presence of carbonate ion [39], whereas some researchers reported that the coexisting anions had an adverse effect on phosphorus adsorption of various adsorbents [40]. In our preliminary experiments, carbonate relatively significantly influenced the phosphate adsorption onto AaN-RM, so it was chosen as the competing ion.

As shown in Fig. 7, carbonate presenting in phosphate solution had a negative effect on the adsorption process. The phosphate adsorption capacity of AaN-RM decreased with the increasing carbonate concentration. When initial carbonate concentration was 206.80 mg/L, the phosphate adsorption capacity decreased by 40.85% compared with that without the existence of carbonate. This is because carbonate occupied the effective adsorption sites on the AaN-RM surface, and increased electrostatic repulsion between the functional group and phosphate, leading to the decrease in phosphate adsorption capacity.

### 3.3. ANN modeling

The data sets of 33 samples were randomly divided into two groups: training and validation subset (25 samples), and testing subset (8 samples). The number of hidden neurons is crucial in ANN modeling, because too many neurons will result in over-fitting, however, a smaller number of neurons may not capture the information adequately [41]. In this paper, the performance of an artificial neural network with varying number of neurons (4–13) in the hidden layer with trainlm algorithm
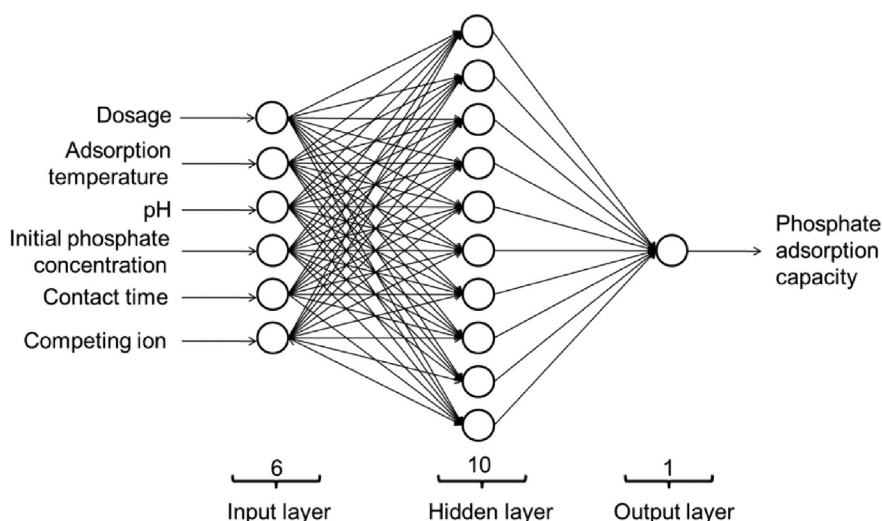


**Fig. 9.** Schematic representation of a (6-10-1) ANN (with six neurons in the input layer, ten neurons in the hidden layer and one neuron in the output layer).

was investigated, and the root mean square error (RMSE) values for the two subsets are shown in Fig. 8. The minimum values of RMSE were obtained when the number of hidden neurons in the hidden layer was 10. Therefore, a 6-10-1 feed forward ANN structure was proposed in this study (Fig. 9).
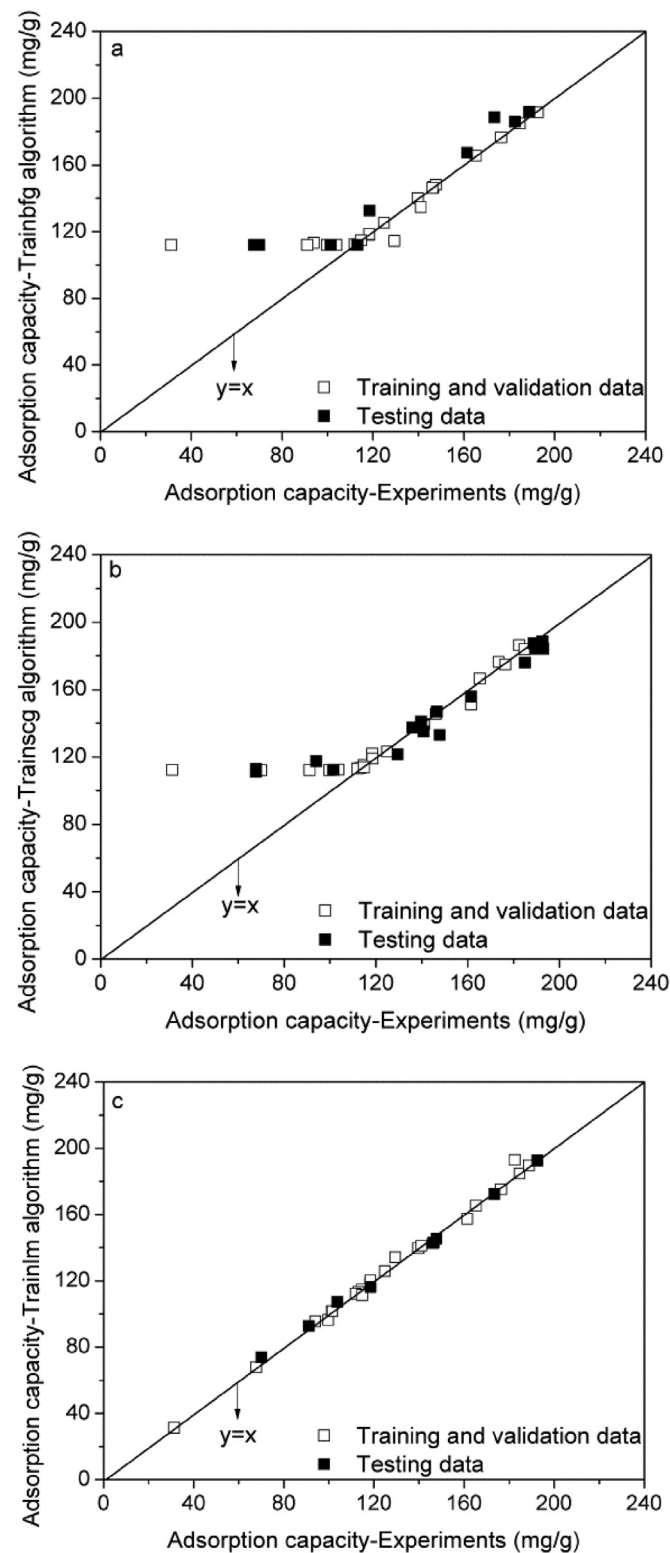


**Fig. 10.** Comparison between experimental and calculated values of the adsorption capacity using ANN with different algorithms (a: trainbfg algorithm; b: trainscg algorithm; c: trainlm algorithm).

Table 4 shows the performance of ANN with different training algorithms. It was found that the trainlm algorithm presented the best solution for the ANN structure of 6-10-1 compared with the trainbfg and trainscg algorithms. In the ANN structure with trainlm algorithm, the RMSE and $R^2$ values for two subsets were 3.06 and 2.61, and 0.9932 and 0.9969, respectively. Fig. 10 illustrated the high correlation between the experimental and predicted values of phosphate adsorption capacity, which apparently confirmed the applicability of ANN with trainlm algorithm to predict the phosphate adsorption performance by AaN-RM.

The importance of each input parameter in the ANN model with trainlm algorithm, which was calculated using Eq. (5), is illustrated in Fig. 11. Among these parameters, contact time and initial phosphate concentration were the most influential parameters on phosphate adsorption by AaN-RM, the importance of which reached 24.64% and 22.16%, respectively. The other parameters also had significant effects on the adsorption process.

## 4. Conclusions

- The phosphate adsorption capacity of AaN-RM decreased with the enhancement of adsorbent dosage, while it increased with the increase of initial phosphate concentration and contact time. The optimal adsorption temperature and initial solution pH for phosphate adsorption onto AaN-RM were 50 °C and 4.0, respectively. Meanwhile, carbonate as the competing ion could greatly increase electrostatic repulsion between the functional group and phosphate, leading to the decrease in phosphate adsorption capacity.

- A 6-10-1 feed forward ANN structure with trainlm algorithm presented the best performance for predicting the phosphate removal by AaN-RM. The RMSE and $R^2$ values for two subsets (training and validation subset, and testing subset) were 3.06 and 2.61, and 0.9932 and 0.9969, respectively.

- The contact time and initial phosphate concentration were the most influential parameters on phosphate removal by AaN-RM according to the importance of different operational parameters in the ANN model with trainlm algorithm, and the importance of which reached 24.64% and 22.16%, respectively.
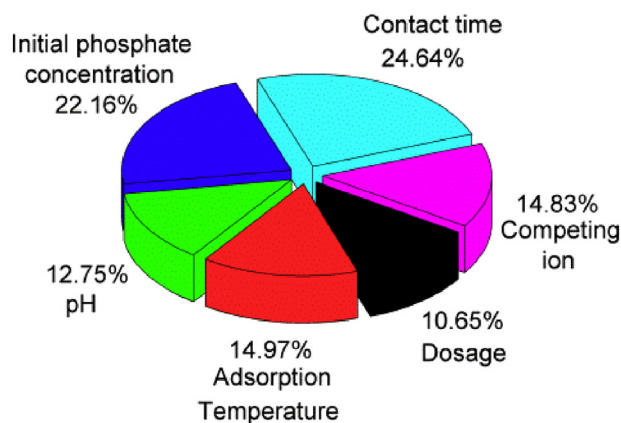
**Fig. 11.** Importance of different operational parameters in the ANN model with trainlm algorithm.

# References

[1] F. Ni, J. He, Y. Wang, Z. Luan, J. Water Process Eng. 6 (2015) 158–165.
[2] M. Arshadi, S. Foroughifard, J. Etemad Gholtash, A. Abbaspourrad, J. Colloid Interface Sci. 452 (2015) 69–77.
[3] H. Zhong, Y. Jiang, G. Zeng, Z. Liu, L. Liu, Y. Liu, X. Yang, M. Lai, Y. He, J. Hazard. Mater. 285 (2015) 383–388.
[4] Y. Dai, Y. Song, X. Tu, Y. Jiang, Y. Yuan, Water Res. 85 (2015) 216–225.
[5] C.J. Liu, Y.Z. Li, Z.K. Luan, Z.Y. Chen, Z.G. Zhang, Z.P. Jia, J. Environ. Sci. 19 (2007) 1166–1170.
[6] Y. Zhao, Q. Yue, Q. Li, X. Xu, Z. Yang, X. Wang, B. Gao, H. Yu, Chem. Eng. J. 193 (2012) 161–168.
[7] Y. Zhao, J. Wang, Z. Luan, X. Peng, Z. Liang, L. Shi, J. Hazard. Mater. 165 (2009) 1193–1199.
[8] W. Liu, X. Chen, W. Li, Y. Yu, K. Yan, J. Clean. Prod. 84 (2014) 606–610.
[9] R. Milačič, T. Zuliani, J. Ščančar, Sci. Total Environ. 426 (2012) 359–365.
[10] S. Wang, H.M. Ang, M.O. Tadé, Chemosphere 72 (2008) 1621–1635.
[11] W. Liang, S.J. Couperthwaite, G. Kaur, C. Yan, D.W. Johnstone, G.J. Millar, J. Colloid Interface Sci. 423 (2014) 158–165.
[12] P. Castaldi, M. Silvetti, G. Garau, S. Deiana, J. Hazard. Mater. 182 (2010) 266–272.
[13] L.M. Despland, M.W. Clark, T. Vancov, D. Erler, M. Aragno, Environ. Sci. Technol. 45 (2011) 5746–5753.
[14] Y.Z. Li, C.J. Liu, Z.K. Luan, X.J. Peng, C.L. Zhu, Z.Y. Chen, Z.G. Zhang, J.H. Fan, Z.P. Jia, J. Hazard. Mater. 137 (2006) 374–383.
[15] V.K. Gupta, S. Sharma, Environ. Sci. Technol. 36 (2002) 3612–3617.
[16] J. Ye, P. Zhang, E. Hoffmann, G. Zeng, Y. Tang, J. Dresely, Y. Liu, Water Air Soil Pollut. 225 (2014) 1–11.
[17] Z. Yıldız, H. Uzun, Microporous Mesoporous Mater. 208 (2015) 50–54.
[18] G.H. Shafabakhsh, O. Jafari Ani, M. Talebsafa, Constr. Build. Mater. 85 (2015) 136–143.
[19] N.G. Turan, B. Mesci, O. Ozgonenel, Chem. Eng. J. 171 (2011) 1091–1097.
[20] B. Dębska, B. Guzowska-Świder, Anal. Chim. Acta 705 (2011) 283–291.
[21] G. Chen, K. Fu, Z. Liang, T. Sema, C. Li, P. Tontiwachwuthikul, R. Idem, Fuel 126 (2014) 202–212.
[22] Q. Wang, Y. Li, M. Diao, W. Gao, Z. Qi, Ocean Eng. 108 (2015) 33–45.
[23] P. Chutia, S. Kato, T. Kojima, S. Satokawa, J. Hazard. Mater. 162 (2009) 440–447.
[24] M. Ghaedi, E. Shojaeipour, A.M. Ghaedi, R. Sahraei, Spectrochim. Acta 142 (2015) 135–149.
[25] K.M. Desai, S.A. Survase, P.S. Saudagar, S.S. Lele, R.S. Singhal, Biochem. Eng. J. 41 (2008) 266–273.
[26] K.P. Singh, A. Basant, A. Malik, G. Jain, Ecol. Model. 220 (2009) 888–895.
[27] J. Ye, X. Cong, P. Zhang, E. Hoffmann, G. Zeng, Y. Wu, H. Zhang, W. Fang, Water Air Soil Pollut. 226 (2015) 306.
[28] Q. Hu, N. Chen, C. Feng, W. Hu, Appl. Surf. Sci. 347 (2015) 1–9.
[29] A.O. Babatunde, Y.Q. Zhao, Y. Yang, P. Kearney, Chem. Eng. J. 136 (2008) 108–115.
[30] J. Liu, L. Wan, L. Zhang, Q. Zhou, J. Colloid Interface Sci. 364 (2011) 490–496.
[31] M. Yang, J. Lin, Y. Zhan, H. Zhang, Ecol. Eng. 71 (2014) 223–233.
[32] B. Riebe, S. Dultz, C. Bunnenberg, Appl. Clay Sci. 28 (2005) 9–16.
[33] B. Schreiber, T. Brinkmann, V. Schmalz, E. Worch, Water Res. 39 (2005) 3449–3456.
[34] J. Pradhan, S.N. Das, R.S. Thakur, J. Colloid Interface Sci. 217 (1999) 137–141.
[35] H. Genc-Fuhrman, J.C. Tjell, D. Mcconchie, Environ. Sci. Technol. 38 (2004) 2428–2434.
[36] S. Gogoi, S.K. Nath, S. Bordoloi, R.K. Dutta, J. Environ. Manag. 152 (2015) 132–139.
[37] J. Ye, X. Cong, P. Zhang, E. Hoffmann, G. Zeng, Y. Liu, W. Fang, Y. Wu, H. Zhang, Appl. Surf. Sci. 356 (2015) 128–134.
[38] Y. Yang, Y.Q. Zhao, A.O. Babatunde, L. Wang, Y.X. Ren, Y. Han, Sep. Purif. Technol. 51 (2006) 193–200.
[39] R. Saad, K. Belkacemi, S. Hamoudi, J. Colloid Interface Sci. 311 (2007) 375–381.
[40] W.Y. Huang, D. Li, Z.Q. Liu, Q. Tao, Y. Zhu, J. Yang, Y.M. Zhang, Chem. Eng. J. 236 (2014) 191–201.
[41] Y.M. Guo, Y.G. Liu, G.M. Zeng, X.J. Hu, W.H. Xu, Y.Q. Liu, S.M. Liu, H.S. Sun, J. Ye, H.J. Huang, Ecol. Eng. 64 (2014) 18–26.